Wear 308 (2013) 35–45

Contents lists available at ScienceDirect

Wear

journal homepage: www.elsevier.com/locate/wear

Rolling contact fatigue resistance of PVD CrN and TiN coated austempered ductile iron

Diego Alejandro Colombo [a,b,*], María Dolores Echeverría [a,b], Sebastián Laino [b], Ricardo Cesar Dommarco [b], Juan Miguel Massone [b]

[a] Mechanical Technology Group, School of Engineering—Universidad Nacional de Mar del Plata, Av. J.B. Justo 4302, B7608FDQ Mar del Plata, Argentina
[b] Metallurgy Division, INTEMA—CONICET, School of Engineering—Universidad Nacional de Mar del Plata, Av. J.B. Justo 4302, B7608FDQ Mar del Plata, Argentina

ARTICLE INFO

Article history:
Received 22 May 2013
Received in revised form
6 September 2013
Accepted 21 September 2013
Available online 14 October 2013

Keywords:
Austempered ductile iron
Surface finishing
Physical vapor deposition
CrN
TiN
Rolling contact fatigue

ABSTRACT

This work studies the rolling contact fatigue (RCF) behavior of PVD CrN and TiN coated ADI samples. The effect of the substrate surface finishing method (grinding and polishing) and coating material on RCF life is also evaluated. Coatings were applied in an industrial reactor. Deposition times were adjusted to obtain similar coating thicknesses in both coating materials. RCF tests were performed in a flat washer type testing rig, using a thrust ball bearing as a counterpart. The maximum contact pressure (p_0) was set at 1000 and 1400 MPa.

The results obtained indicate that the RCF tests performed at $p_0 = 1000$ MPa cause no failures on the samples analyzed, while those performed at $p_0 = 1400$ MPa cause failures in both uncoated and coated samples. Failures in coated samples are mainly characterized by coating delamination and, to a lesser extent, by spall formation in the substrate. Graphite nodules present on the substrate surface act as preferential sites for coating fracture and subsequent delamination. The RCF resistance of coated samples is lower than that of uncoated samples regardless of the substrate surface finishing method employed. The surface hardening produced by the abrasive cutting of grinding improves the RCF resistance of the uncoated and coated samples.

1. Introduction

Austempered ductile iron (ADI) is increasingly being used for the manufacturing of mechanical components given the wide range of mechanical properties achievable after the proper adjustment of the chemical composition and heat treatment parameters, as well as its advantageous features if compared to high-strength cast steels, such as its lower cost and weight, greater flexibility in parts design and comparable tensile strength [1–3]. Most of the production is used satisfactorily in elements subjected to dynamic and cyclic loads, i.e., fatigue and also rolling contact fatigue (RCF) [4–6].

Several authors have studied the rolling contact fatigue (RCF) behavior of ADI with different nodule counts (150–1400 nod/mm^2) and austempering temperatures (240–360 °C) [7–11]. They found that ADI resistance to RCF increases as austempering temperature decreases and nodule count increases. A decrease in surface roughness also increases RCF resistance of ADI. Surface and subsurface graphite nodules act as preferential sites for crack nucleation. Consequently, the use of surface treatments could offset the negative effect of the surface nodules. However, any surface treatment involving ADI exposure to high temperature during long periods may cause changes in the ausferritic microstructure and negatively affect its mechanical properties [12].

During the last decade, significant advances have been made in the application of PVD coatings of different materials on ADI substrates. Several authors have accounted for improvements in high cycle fatigue resistance, corrosion resistance and hardness [13–16]. More recent studies have reported that duplex treatments (electroless nickel and CrTiAlN PVD coating) provide better performance against erosive wear than monolithic coatings do and even reduce ADI friction coefficient [17]. In all the studies, processing temperatures of up to 300 °C were used and no deterioration of ADI microstructure was reported.

Moreover, the authors of the present work found a combination of industrial-use processing parameters producing PVD TiN and CrN coatings of acceptable characteristics as far as coating thickness, hardness, residual stresses and adhesion are concerned, causing no significant deterioration of ADI microstructure. Additionally, the analysis of the effects of the substrate characteristics on coating properties evidenced little influence of the austempering temperature and nodule count [18–20].

* Corresponding author at: Mechanical Technology Group, School of Engineering —Universidad Nacional de Mar del Plata, Av. J.B. Justo 4302, B7608FDQ Mar del Plata, Argentina. Tel.: +54 223 481 6600x260; fax: +54 223 481 0046.
E-mail address: diegocolombo@fi.mdp.edu.ar (D.A. Colombo).

0043-1648/$ - see front matter © 2013 Elsevier B.V. All rights reserved.
http://dx.doi.org/10.1016/j.wear.2013.09.015

Grinding is one of the most commonly used processes in the industry when it comes to surface finishing of mechanical components. The abrasive cutting of grinding produces plastic deformation and high temperatures in the workpiece-wheel contact area, depending on the workpiece material, wheel characteristics and grinding variables such as workpiece speed, wheel speed and depth of cut per pass. As a result, surface hardening and residual stresses are generated, which may affect the service behavior of the components whether coated or not.

To the best of the authors' knowledge, there is no information available regarding the RCF behavior of PVD coated ADI samples, nor about the effect of the substrate surface finishing method and coating material on RCF life. On this basis, the aim of this work is to study the RCF performance of PVD CrN and TiN coated ADI with different surface finishing methods (grinding and polishing).

2. Experimental procedures

2.1. Substrate material and samples preparation

The ductile iron utilized in this work was produced in a 55 kg middle-frequency induction furnace (3 KHz). The melt was conventionally nodulized and inoculated [18] and then it was poured into horizontal sand molds designed to obtain 70 mm diameter and 10 mm thick discs.

The chemical composition of the material (wt%), analyzed by optical emission spectrometry, was as follows: C=3.35; Si=2.87; Mn=0.13; S=0.015; P=0.032; Mg=0.043; Cu=0.76; Ni=0.57 and Fe balanced. The carbon equivalent was eutectic (CE=4.32). Based on chart comparisons, nodularity exceeded 90% in all casting thicknesses.

Discs were cut and machined by turning, in order to obtain the test samples illustrated in Fig. 1.

Afterwards samples were subjected to an austempering heat treatment, consisting in austenitising at 910 °C for 120 min, austempering in a salt bath at 280 °C for 90 min, and subsequently air cooling to room temperature. According to the aforementioned, a high resistance substrate (i.e., a low austempering temperature) was selected to evaluate the RCF behavior of the PVD coated ADI samples.

2.2. Samples surface finishing

The treated samples were subjected to two different surface finishing methods: manual polishing and grinding.

Conventional surface grinding was carried out on a horizontal-spindle (peripheral) surface grinder under industrial-use cutting conditions. Three roughing passes and one finishing pass were conducted on each sample. The finishing pass aims to attain low surface roughness. A vitrified wheel with SiC abrasive grains, identified as IC36/46I/J5V9, was employed. A 5% aqueous solution of soluble oil "Dromus B" was used as cooling fluid.

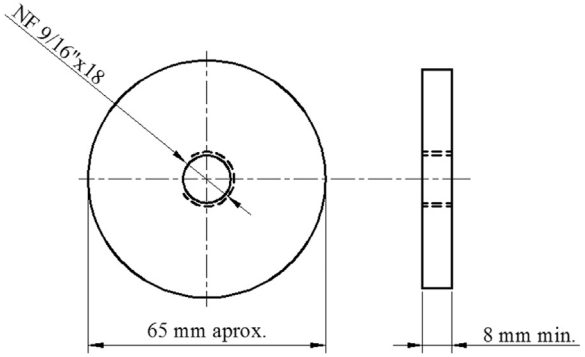

Fig. 1. Scheme of the RCF sample geometry and dimensions.

Table 1
Deposition parameters of CrN and TiN coatings.

Coating material	CrN	TiN
Substrate-target distance [mm]	200	200
Substrate BIAS voltage [V]	−175	−175
Arc current [A]	60	60
Chamber pressure [Pa]	2	1.5
Substrate temperature [°C]	300	300
Deposition time [min]	150	180

Manual polishing was performed using SiC waterproof paper. The final grit size was adjusted to obtain a similar arithmetic average roughness (Ra) for both surface finishing methods. It was found that a progressive polishing of up to 220 grit size fulfilled this requirement.

2.3. PVD coating process

CrN and TiN coatings were applied by arc ion plating (AIP) in an industrial reactor using sets of processing parameters specifically designed for ADI. Prior to this, the samples had been thoroughly degreased, ultrasonically cleaned, rinsed with alcohol and dried with warm air. Inside the chamber, and prior to deposition, samples were cleaned once again by bombardments with energetic ions. Table 1 lists the process parameters used. The deposition times were adjusted to obtain similar coating thicknesses for both coatings materials.

2.4. Substrates and coatings characterization

Samples average nodule count was determined by optical microscopy and digital image processing, taking a 5 μm diameter nodule as threshold value. The average nodule count obtained was 497 nod/mm^2.

Phase identification and residual stress measurements in the uncoated and coated samples were performed by x-ray diffraction (XRD). A Phillips XPERT-PRO diffractometer was utilized, with Cu Kα radiation (λ=1.54187 Å) at 40 kV and 40 mA. XRD patterns for phase identification were recorded in a 2θ range from 30° to 90° in steps of 0.02° and with a counting time of 1 s per step.

Stress measurements were conducted using the $\sin^2\psi$ method, with the assumption of a biaxial stress state. The optimal diffraction peaks for measurements on the coated samples were CrN and TiN (422). The 2θ angle ranged from 125° to 135° for CrN and from 120° to 132° for TiN, with a 2θ step of 0.05° and 5 s per step. The peak profiles were recorded at ψ tilt angles of 0°, 25.29°, 37.17°, 47.73° and 58.69°, respectively.

The optimal diffraction peak for measurements on the uncoated samples was Fe-α (222). The 2θ angle ranged from 134° to 140°, with a 2θ step of 0.05° and 5 s per step. The peak profiles were recorded at ψ tilt angles of 0°, 26.57°, 39.23°, 50.77° and 63.44° respectively.

The x-ray elastic constants (XEC's) used to calculate the stresses in the uncoated and coated samples were extracted from bibliographic data [21–23].

The conventional arithmetic average roughness (*Ra*) of the uncoated and coated samples was analyzed using a stylus profilometer (Taylor Hobson Surtronic 3+) with a 4 mm evaluation length (cut-off, 0.8 mm). In addition, optical microscopy was utilized for the surface characterization of the samples surface.

Coatings thickness was measured on fractured cross sections micrographs, obtained by SEM (JEOL JSM-6460LV).

Knoop microhardness (15 g load) of the uncoated and coated samples was determined using a microhardness tester.

Coating adhesion was evaluated by the Rockwell-C adhesion test (150 kg load), using a universal hardness tester [24].

2.5. RCF tests

RCF tests were performed in a flat washer type testing rig. In this type of test, a disk shaped sample (Fig. 1) is run against the balls of a thrust ball bearing at a velocity ω and under a normal load P, using lubricated, pure rolling conditions. Fig. 2 provides a schematic view of the testing rig.

Two thrust ball bearings with different nominal diameters were used as a counterpart so as to be able to conduct two tests per sample side, thus diminishing the number of samples required. The spindle rotation speed was 1650 rpm. Table 2 lists the characteristics of the bearings employed.

According to a previous study [25], the samples were tested at p_0 values of 1000 and 1400 MPa. The corresponding normal loads and contact radii were calculated according to the elastic Hertz theory as a reference, even though some plastic deformation could be present. Table 3 lists the geometric and elastic properties of the ADI samples and loading balls utilized.

The normal loads required to apply the aforementioned p_0 values on the uncoated samples are reported in Table 4.

Based on other studies [26–28], pressure distribution in the contact region on coated samples depends on contact radius (a) and coating thickness (t). For ratios $t/a \to 0$ and $t/a \to 1$, pressure distribution could be determined using the Hertz theory and the elastic properties of substrates and coatings, respectively.

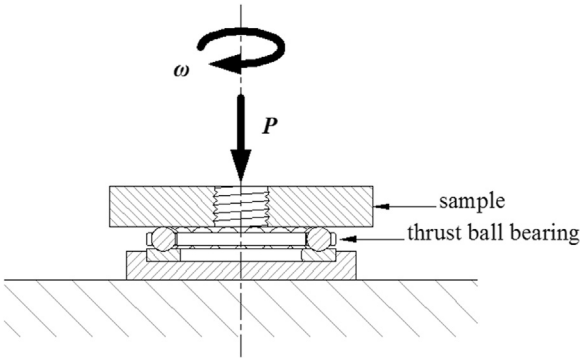

Fig. 2. Schematic view of the RCF testing rig.

Table 2
Characteristics of the counterparts employed.

Designation	Ball diameter [mm]	Number of balls	Rolling diameter [mm]	Loading frequency [cycles/h]
51106	6	18	38.5	891,000
51107	6	21	44	1,039,500

Table 3
Geometric and elastic properties of ADI samples and loading balls.

Element	Material	Radius of curvature [m]	Poisson's ratio	Elastic modulus [GPa]
Ball	SAE 52100	0.003	0.3	210
Sample	ADI	∞	0.25	170

Table 4
Normal loads required to apply p_0 values of 1000 and 1400 MPa on uncoated samples.

p_0 [MPa]	Counter part	P [N]
1000	51106	82
	51107	95
1400	51106	223
	51107	260

On the other hand, it comes out that the contact pressure can differ significantly from Hertz distribution when the ratio t/a varies between these two limit cases. This deviation is enhanced when the ratio of the reduced modulus of the substrate to that of the coating increases.

In this study, the contact radii generated are close to 46 and 65 μm. These values are significantly higher than those of the coating thickness (t) of coated samples, and, as a consequence, the calculated normal loads are valid for both uncoated and coated samples.

The specific oil coating thickness parameter (λ) can be calculated with the following expression:

$$\lambda = \frac{h_0}{\sqrt{Ra_1{}^2 + Ra_2^2}}$$

where h_0 is the minimum oil coating thickness and Ra_1 and Ra_2 the arithmetic average roughness of the contact surfaces, i.e., the sample and loading balls.

The minimum oil coating thickness was calculated using the Hamrock and Dowson equation [29]. Depending on the couple sample-counterpart analyzed, the testing conditions produce λ values in the range 1.22–1.74, thereby promoting microasperities interaction.

In the RCF tests, the machine is continuously run until a macroscopic fatigue failure is produced on the sample surface. Such failure in the rolling track (RT) causes an increase in the vibration level, which is measured by a highly sensitive accelerometer. When the vibration level exceeds a preset value, the test is automatically stopped. The life to failure of the samples is measured by an hour meter and then converted into loading cycles. On the other hand, when the test duration exceeds 100 h ($\sim 100 \times 10^6$ loading cycles) without causing failures in the sample surface, the machine is stopped resulting in a suspension.

Several RCF tests were carried out for each sample variant. The RT of the tested samples was examined by using SEM and stylus profilometry. Fatigue tests results were analyzed using the two-parameter Weibull distribution. L_{10}, L_{50} and characteristic (η) lives were evaluated.

3. Results and discussion

3.1. Substrates and coatings characteristics

Table 5 lists the characteristics of the uncoated and coated samples.

As it can be noticed, according to what was intended, the Ra values of the uncoated samples are similar for both surface finishing methods. On the other hand, the deposition processes alter the surface roughness of the samples, leading to a small increase in Ra.

Fig. 3 shows surface micrographs of the polished and ground samples before and after coating deposition. With respect to the uncoated polished samples (Fig. 3a), the presence of surface nodules can be noticed, with some of them presenting partial or

Table 5
Characteristics of the uncoated and coated samples.

Surface finishing	Sample	*Ra* [μm]	Coating thickness [μm]	Microhardness [$HK_{0.015}$]	Residual stresses [GPa]
Polished	ADI	0.192 ± 0.025	–	375 ± 55	−0.95 ± 0.04
	ADI–CrN	0.229 ± 0.029	2.46 ± 0.36	1529 ± 90	−3.34 ± 0.10
	ADI–TiN	0.232 ± 0.021	2.42 ± 0.60	2372 ± 104	−5.95 ± 0.14
Ground	ADI	0.191 ± 0.028	–	723 ± 87	−0.66 ± 0.03
	ADI–CrN	0.226 ± 0.020	2.38 ± 0.12	1873 ± 99	−3.27 ± 0.11
	ADI–TiN	0.231 ± 0.018	2.51 ± 0.52	2796 ± 121	−5.94 ± 0.13

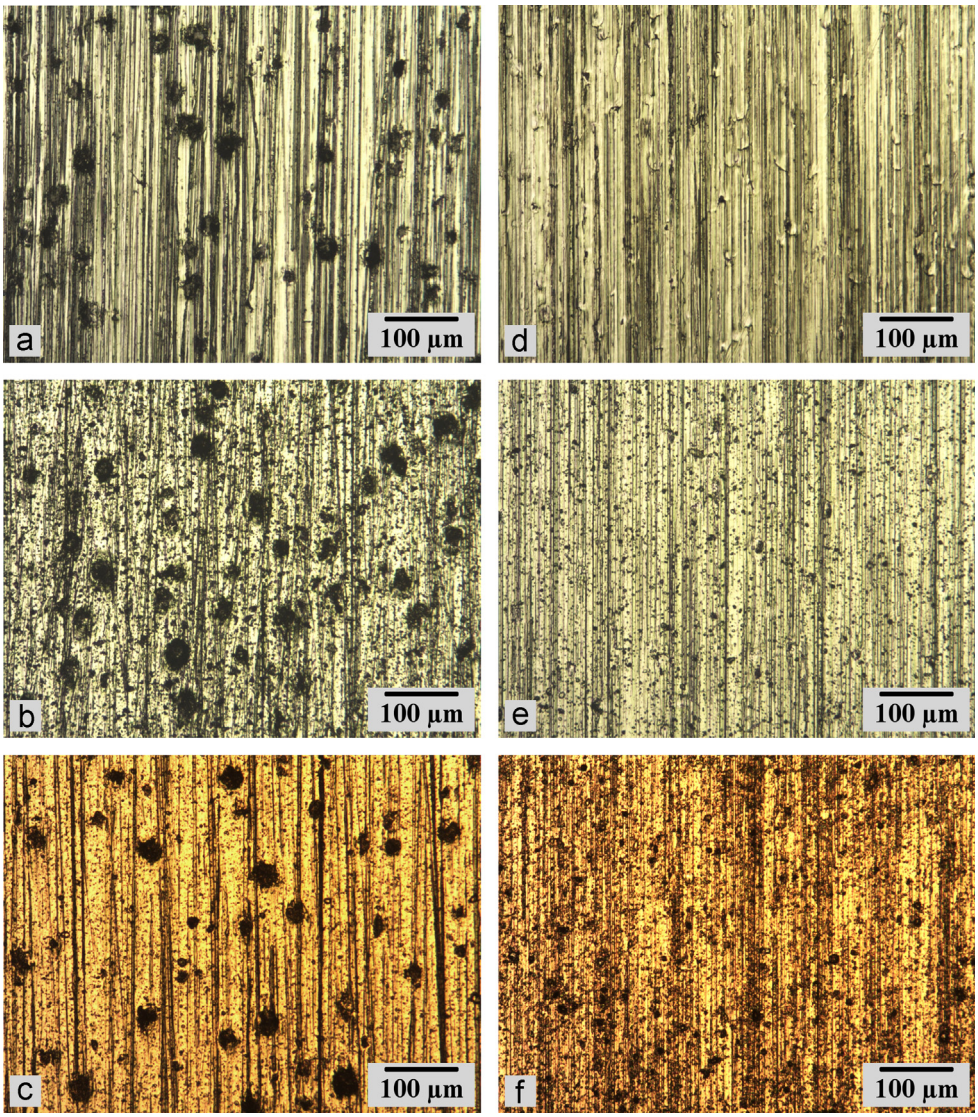

Fig. 3. Samples surface micrographs before and after coating deposition: (a) ADI polished, (b) ADI polished–CrN, (c) ADI polished–TiN, (d) ADI ground, (e) ADI ground–CrN, and (f) ADI ground–TiN.

complete graphite removal [18]. As regards coated polished samples (Fig. 3b and c), only those nodules presenting graphite removal can be seen, since they appear as dark points due to an optic effect. In the ground samples (Fig. 3d–f), nodules cannot be seen at the surface. According to a previous study [11], this feature is ascribed to the plastic deformation of the metallic matrix, inherent to abrasive cutting of grinding, which covers the nodules.

As expected, coating thickness is also similar for both coatings materials.

The Knoop microhardness of the uncoated and coated samples varies with the surface finishing method employed. Ground samples yield higher values due to the surface hardening produced by the abrasive cutting. According to the literature, the values of the CrN coated samples are lower than those of the TiN coated ones.

The residual stresses (RS) of the uncoated samples are compressive and vary with the surface finishing method employed. The RS values of polished samples are higher than those of ground samples. The RS of coated samples are also compressive and do not vary with the different surface finishing methods employed. The RS values of the CrN coated samples are significantly lower than those of the TiN coated ones. Based on a previous report [20], the

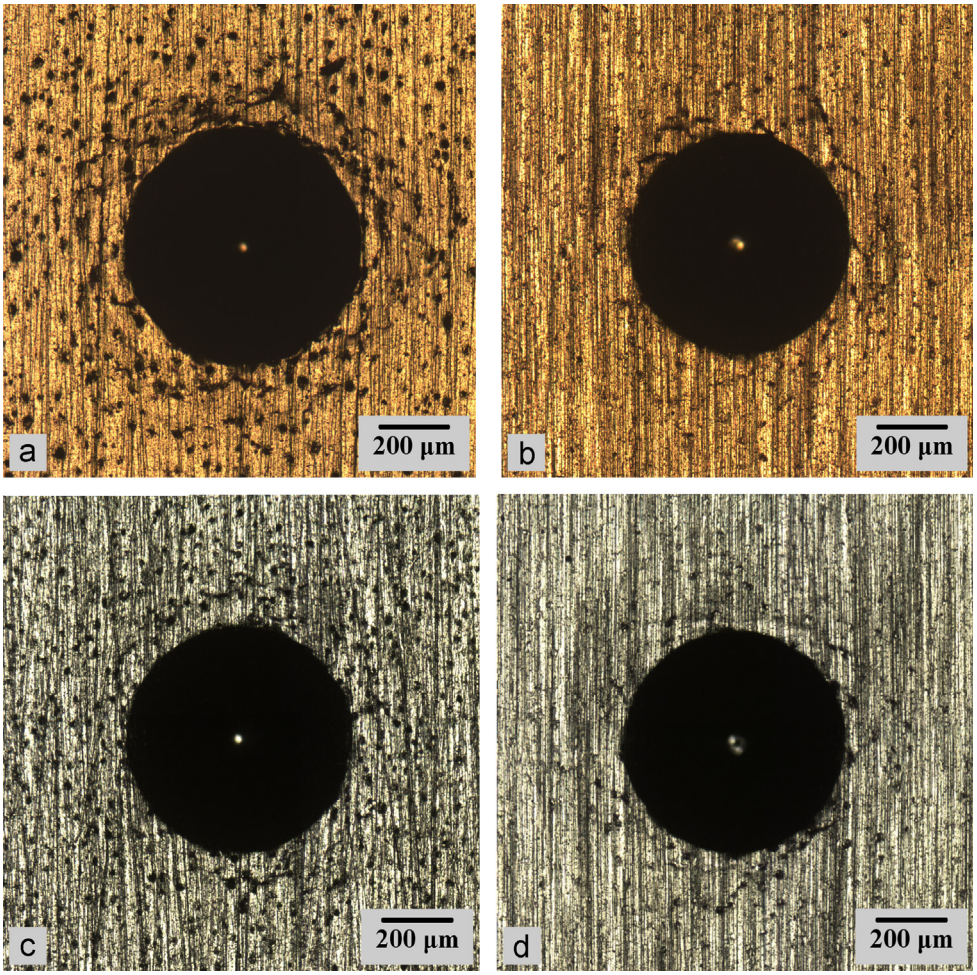

Fig. 4. Imprints on coated samples after Rockwell-C adhesion test: (a) ADI polished–TiN, (b) ADI ground–TiN, (c) ADI polished–CrN, and (d) ADI ground–CrN.

RS of uncoated and coated samples do not change by varying the measurement direction on the sample surface, thus indicating rotationally symmetric biaxial stress states.

The adhesion strength quality of CrN and TiN coatings to polished and ground substrates, as determined by the Rockwell-C adhesion test, can be classified as HF1. No delaminations occurred. Fig. 4 illustrates the imprints resulting from the Rockwell-C adhesion test.

Certain influence of the substrate surface finishing method on the cracking patterns of the coatings can be noted, since polished samples with uncovered surface nodules exhibit a greater number of cracks around the imprints. In agreement with a previous report [18], the cracks propagate mainly among the surface nodules generating circumferential patterns.

3.2. RCF behavior

The p_0 values applied to the test samples should be high enough so as to cause material degradation by microplasticity, though not that high so as to cause material build up along the edges of the RT and, consequently, a modification of the contact geometry, which would invalidate the results.

A simple way to analyze if the contact load is excessive is by examining the RT topography by means of stylus profilometry, as shown in Fig. 5 for the uncoated and coated samples tested at $p_0 = 1400$ MPa after $\sim 20 \times 10^6$ loading cycles.

The profiles obtained do not reveal material build up at the edges of the rolling tracks. Besides, the RT width is various orders of magnitude higher than its depth, indicating that the deformation produced by the contact load is minimal and, consequently, that the results are valid.

Fig. 5 also shows that the RT depth of the uncoated and coated ground samples is lower than that of the polished ones. This behavior is attributed to the surface hardening produced by the abrasive cutting of grinding.

3.2.1. Tests performed at $p_0 = 1000$ MPa

The RCF tests performed at p_0 values of 1000 MPa do not cause failures on the samples analyzed. Fig. 6 shows surface micrographs of an uncoated polished sample.

It can be seen no failures on the sample surface after $\sim 100 \times 10^6$ loading cycles (Fig. 6a). On the other hand, by comparing the sample surface morphology inside and outside the RT (Fig. 6b and c, respectively) it can be noted some alteration of the surface on the RT. This feature is ascribed to the microasperities interaction of the contact bodies, according to the λ values obtained in the theoretical calculations.

Fig. 7 shows surface micrographs of a TiN coated ground sample.

It can be seen several small failures after $\sim 100 \times 10^6$ loading cycles that were not enough to stop the test (Fig. 7a). Moreover, no significant differences between the sample surface morphology inside and outside the RT are observed (Fig. 7b and c, respectively). This feature is ascribed to the high hardness of the TiN coating as compared to ADI.

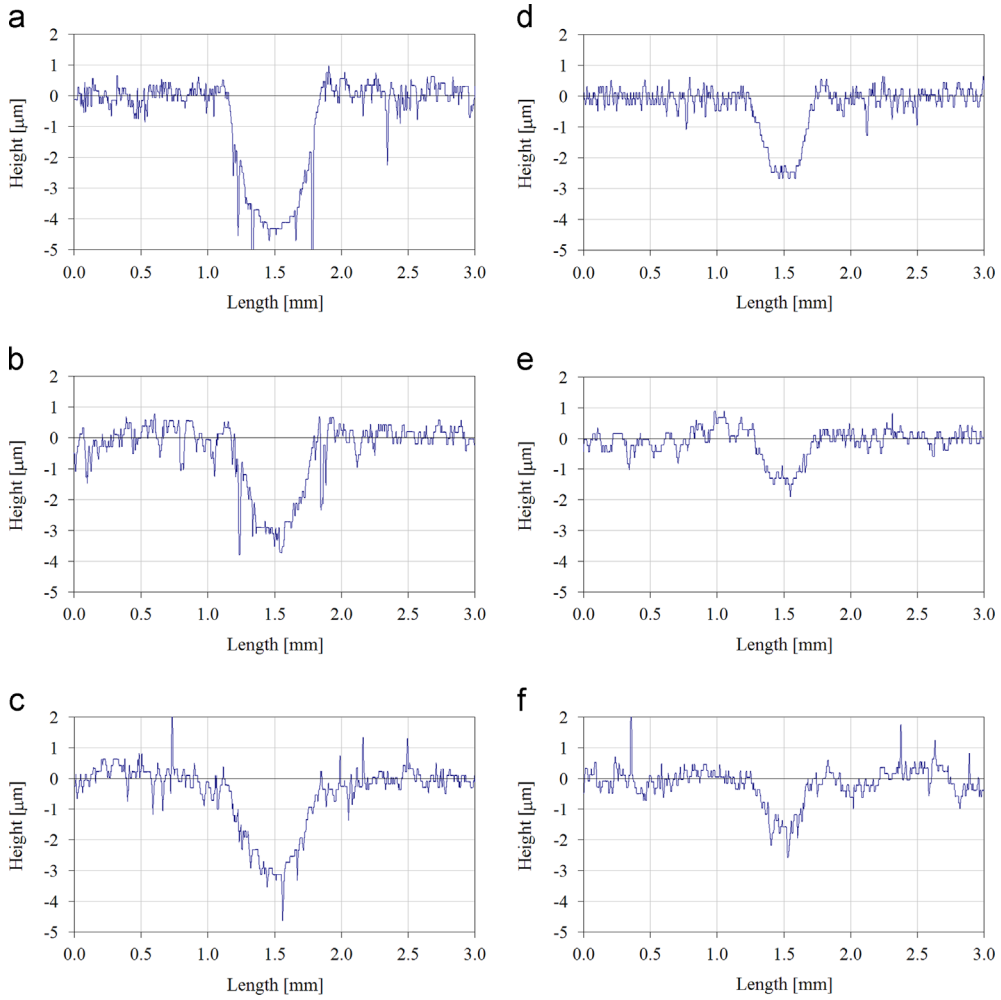

Fig. 5. Rolling track profiles of uncoated and coated samples tested at $p_0 = 1400$ MPa after $\sim 20 \times 10^6$ loading cycles: (a) ADI polished, (b) ADI polished–CrN, (c) ADI polished–TiN, (d) ADI ground, (e) ADI ground–CrN, and (f) ADI ground–TiN.

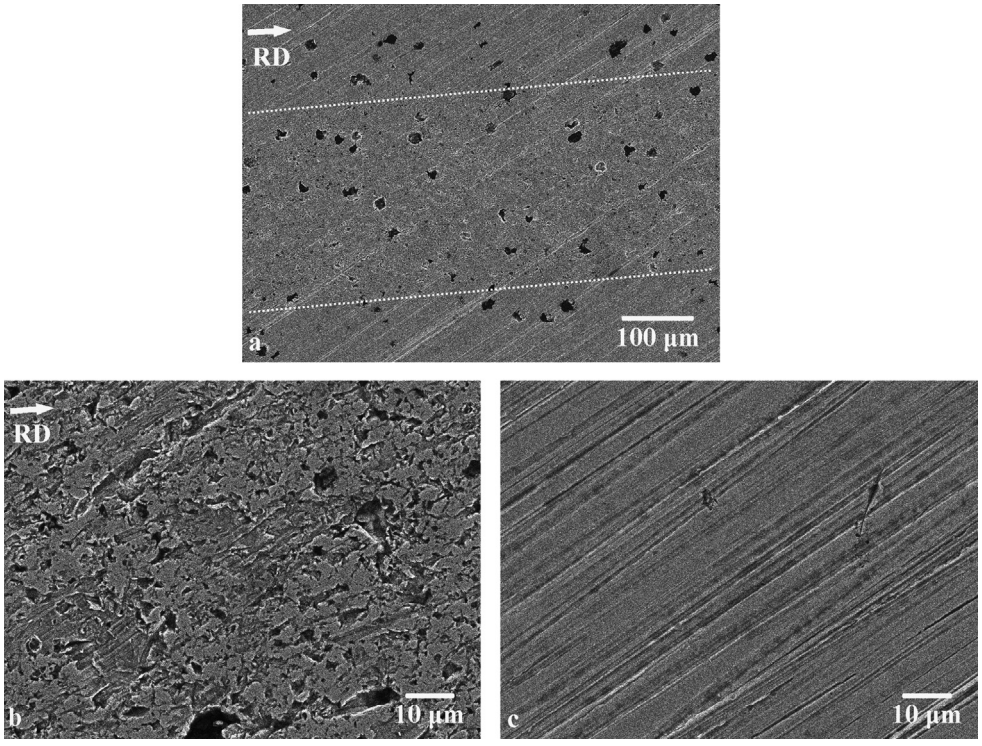

Fig. 6. SEM surface micrographs of an uncoated polished sample: (a) RT after $\sim 100 \times 10^6$ loading cycles, (b) surface morphology inside the RT, and (c) surface morphology outside the RT.

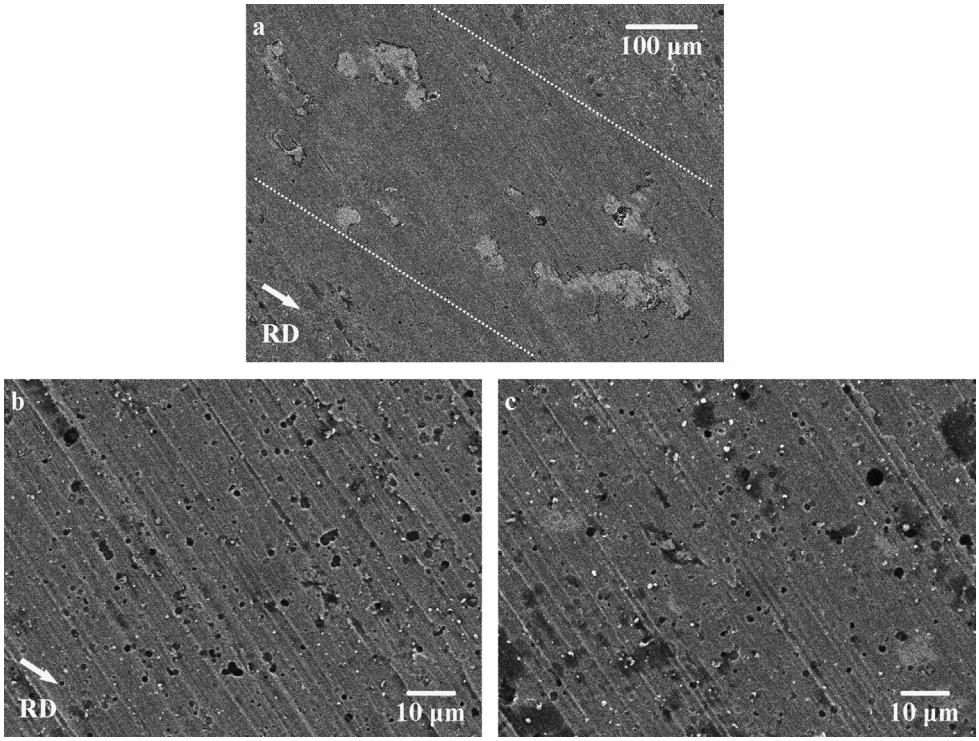

Fig. 7. SEM surface micrographs of a TiN coated ground sample: (a) RT after $\sim 100 \times 10^6$ loading cycles, (b) surface morphology inside the RT, and (c) surface morphology outside the RT.

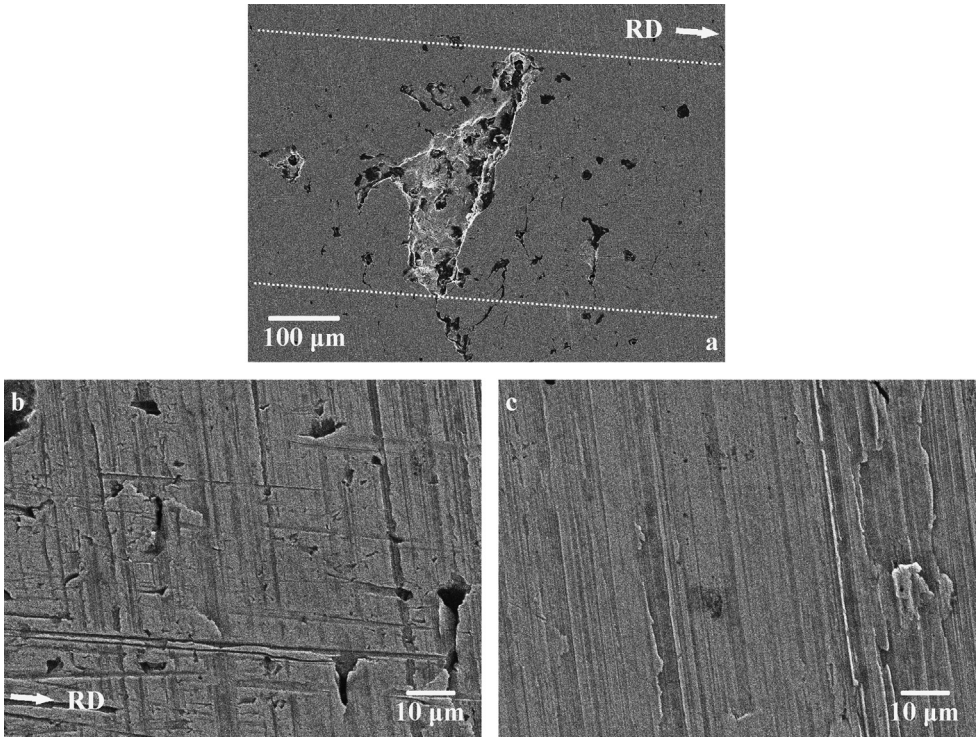

Fig. 8. SEM surface micrographs of an uncoated ground sample: (a) typical RCF failure, (b) surface morphology inside the RT, and (c) surface morphology outside the RT.

3.2.2. Tests performed at $p_0 = 1400$ MPa

The RCF tests performed at p_0 values of 1400 MPa cause failures on the uncoated and coated samples. Fig. 8 shows surface micrographs of an uncoated ground sample.

A typical V shaped RCF failure, called spall, at the RT of the uncoated ground sample, pointing opposite to the rolling direction (RD) is illustrated in Fig. 8a. In agreement with previous reports [7,10], it can be seen that propagating cracks follow a path connecting surface and subsurface nodules. In addition, some scratches inside the RT oriented along the RD can be observed (Fig. 8b), due to the microasperities interaction of the contact bodies.

The examination of the rolling tracks on the coated samples revealed two different failure modes. The first and the most

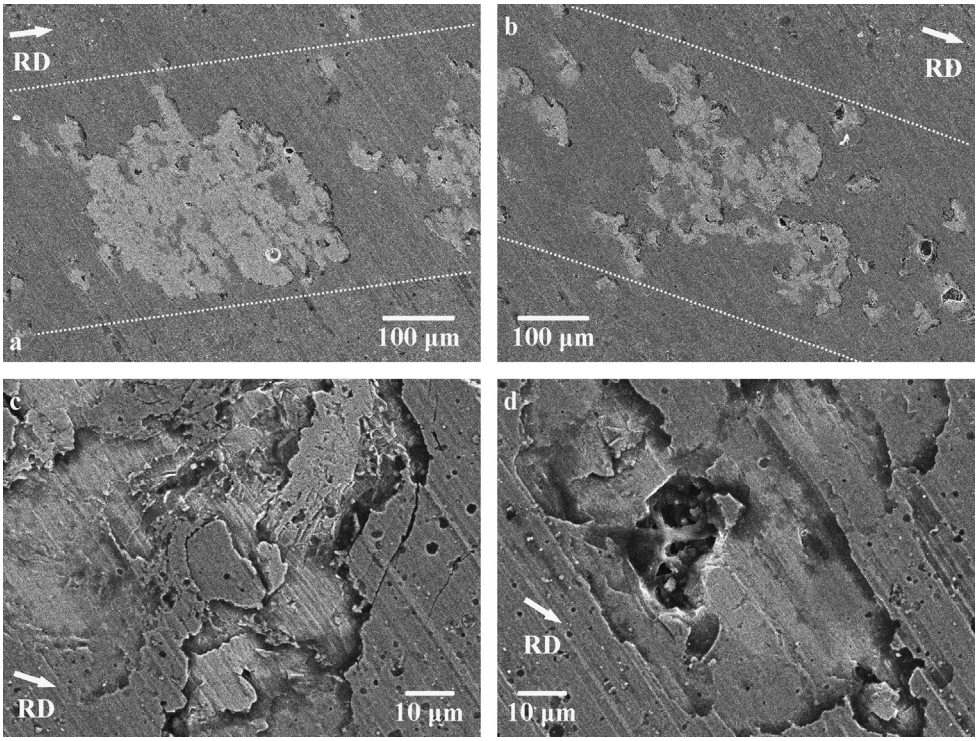

Fig. 9. RCF failures on coated samples characterized by coating fracture and delamination: (a) and (b) ADI ground–TiN, (c) and (d) substrate grinding scratches in the delaminated areas.

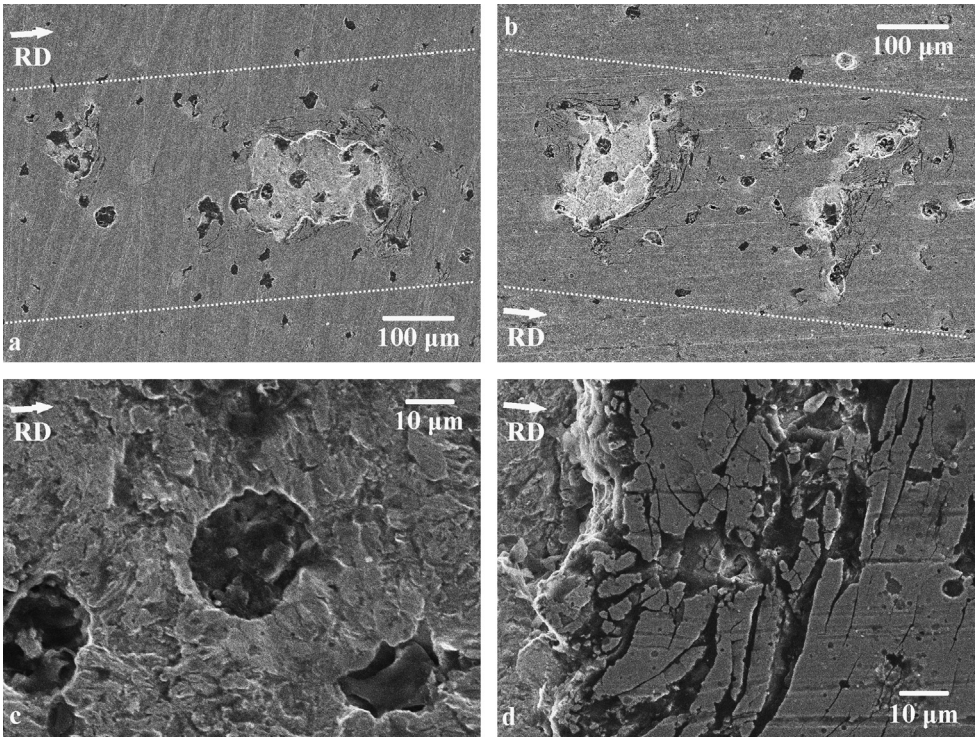

Fig. 10. RCF failures on coated samples characterized by spall formation in the substrate: (a) ADI polished–CrN, (b) ADI polished–TiN, (c) substrate fracture surface inside the spall, and (d) coating cracking network on the edges of the spall.

predominant one is the fracture and subsequent delamination of the coating without loss of substrate material, as shown in Fig. 9, while the second and less prevalent one is the spall formation in the substrate, as shown in Fig. 10. Both types of failures have been observed by other authors in PVD coated samples [30–32].

It was also observed that the surface nodules act as preferential sites for coating fracture and delamination, as illustrated in Fig. 11. This behavior is consistent with a previous report referred to RCF cracking mechanisms observed in ADI [8], which states that in those graphite nodules that are located close to the surface, the

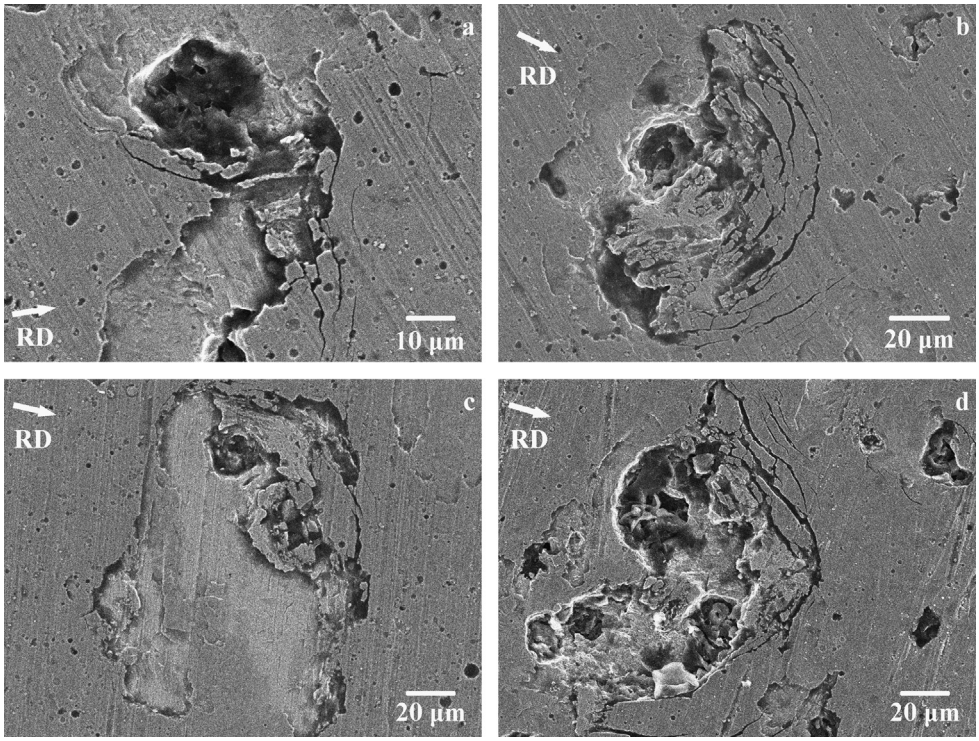

Fig. 11. Coating delamination around graphite nodules on the coated samples: (a) and (b) ADI ground–CrN, (c) ADI ground–TiN, and (d) ADI polished–CrN.

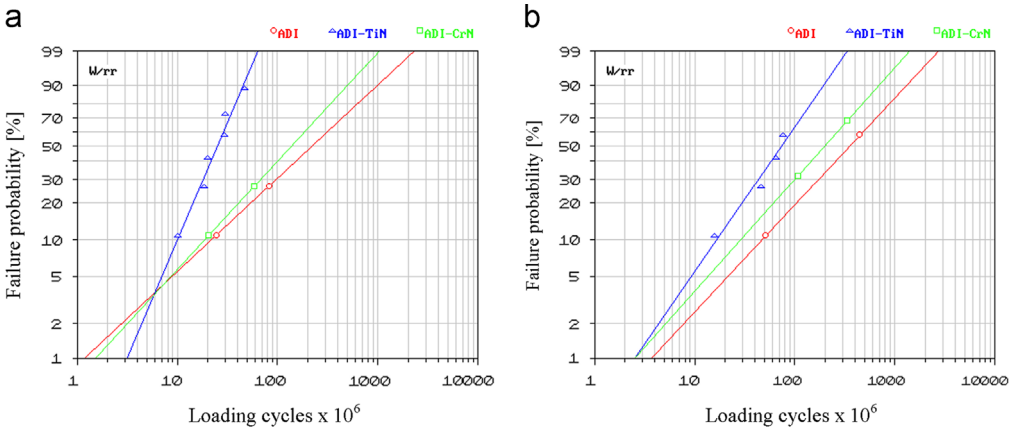

Fig. 12. Weibull plots of uncoated and coated samples for the different surface finishing methods analyzed: (a) polishing and (b) grinding.

thin layer of material above them is broken during the tests and graphite tends to be expelled leaving empty cavities. In the case of coated ADI samples, it is believed that this mechanism initiates the fracture and delamination of the coating and promotes its subsequent expansion to neighboring nodules.

The Weibull plots of the uncoated and coated samples for the different surface finishing methods analyzed are shown in Fig. 12. The figure depicts the failure probability (ordinate) vs. the number of loading cycles (abscissa). The results of the Weibull analysis are summarized in Table 6, reflecting L_{10}, L_{50} and η lives. Other parameters such as Weibull slope (β) and the coefficient of determination (R^2) are also provided.

In order to analyze the results of the RCF tests by using the two-parameter Weibull distribution, it is necessary to have at least two unsuspended data for each group of tested samples. The uncoated and CrN coated ground samples did not meet this requirement. For that reason, some of the suspended tests, i.e., those reaching $\sim 100 \times 10^6$ loading cycles without failures, were continued until failure occurrence.

It can be seen that the L_{10}, L_{50} and η lives of the CrN and TiN coated samples are lower than those of the uncoated ones. The deposition of CrN and TiN decreases the RCF life of the polished samples by 42.5% and 91.6%, respectively, and that of the ground samples by 45.0% and 81.2%, respectively. This behavior is attributed to the negative influence exerted by the surface nodules, which act as preferential sites for coating delamination. Coating thickness could also negatively affect the RCF behavior of the coated samples. According to other studies [25,33–36], coating thicknesses higher than 1 µm do not improve the RCF life of steel samples coated with TiN by PVD techniques for contact pressures greater than 1100 MPa.

Additionally, the L_{10}, L_{50} and η lives of the ground samples are higher than those of the polished ones. Grinding increases the η life of the uncoated samples by 48.4%, while that of the CrN and

Table 6
Results of Weibull analysis.

Surface finishing	Sample	L_{10} [cycles × 10^6]	L_{50} [cycles × 10^6]	η [cycles × 10^6]	β	R^2
Polished	ADI	21.76	224.25	353.05	0.81	0.999
	ADI–CrN	18.45	137.40	203.07	0.94	0.999
	ADI–TiN	9.85	24.82	29.71	2.04	0.968
Ground	ADI	46.29	352.81	523.79	0.93	0.999
	ADI–CrN	28.08	197.31	288.33	0.97	0.999
	ADI–TiN	16.25	73.50	98.58	1.25	0.955

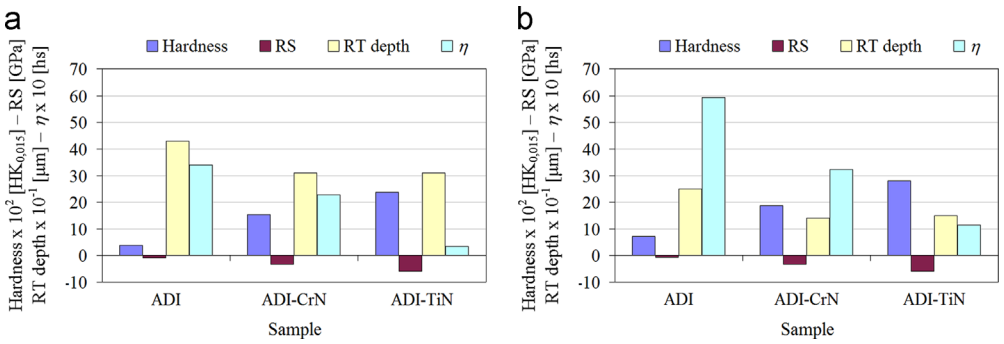

Fig. 13. Relationship between hardness, RS, RT depth and characteristic life of uncoated and coated samples: (a) polished and (b) ground.

TiN coated samples by 42.0% and 231.8%, respectively. This behavior is ascribed to the surface hardening caused by the plastic deformation associated to the abrasive cutting of grinding, which improves the properties gradient between substrate and coating. Another factor worthy of consideration is the lack of craters in the ground surfaces, which can assume the effect of stress concentrators, and thus promote earlier failures.

Fig. 13 relates the hardness and RS of the uncoated and coated samples to the RT depth and characteristic life, for the different surface finishing methods analyzed.

For both surface conditions, it can be seen that a higher difference in the hardness and RS values between the uncoated and coated samples produces a clear decrease in the η life of the latter, while the RT depth does not vary significantly. This behavior is attributed to the abrupt change of properties between substrates and coatings. This change is more significant in the TiN coated samples which, in turn, presented the lowest RCF life. Consequently, the application of multilayer coatings could enhance ADI RCF resistance by modifying, on the one hand, the properties gradient between substrate and coating and, on the other, by masking the surface nodules with a first layer of a given material.

It is worth mentioning that the results of the Rockwell-C adhesion tests contrast those obtained in the FCR test. In the former no delaminations occurred while in the latter failures were mainly characterized by coating delamination. This behavior is ascribed to the different stress states generated in each test. On the other hand, in both tests, the surface nodules act as preferential sites for failure formation, either coating cracking or delamination.

4. Conclusions

The RCF tests performed at $p_0 = 1000$ MPa do not cause failures on the samples analyzed while tests performed at $p_0 = 1400$ MPa cause failures in the uncoated and coated samples.

Failures in CrN and TiN coated samples are mainly characterized by coating delamination and, to a lesser extent, by the spall formation in the substrate. Graphite nodules present on the substrate surface act as preferential sites for coating fracture and subsequent delamination.

The RCF resistance of the coated samples turned out to be lower than that of the uncoated samples for the different substrate surface finishing methods employed. The deposition of CrN and TiN decreases the characteristic life of the polished samples by 42.5% and 91.6%, respectively, and that of the ground samples by 45.0% and 81.2%, respectively.

The surface hardening caused by the plastic deformation associated to the abrasive cutting of grinding improves the RCF resistance of the uncoated and coated samples.

A greater gap between substrate and coating properties produces a lower RCF resistance, as in the case of the TiN coated samples.

The application of multilayer coatings could improve ADI RCF resistance by modifying, on the one hand, the properties gradient between substrate and coating and, on the other, by masking the surface nodules with a first layer of a given material. Coating thicknesses less than 1 µm could also be favorable.

Acknowledgments

The authors wish to thank the company Sudosilo S.A. for its generous collaboration in coatings deposition.

References

[1] R.A. Martinez, R.E. Boeri, J.A. Sikora, Impact and fracture properties of ADI, compared with SAE 4140 steel, Trans. Am. Foundry Soc. 106 (1998) 27–30.
[2] J.R. Keough, ADI: ideal for high-strength, high-wear applications, Eng. Cast. Solut. 3 (2001) 42–44.
[3] P. David, J. Massone, R. Boeri, J. Sikora, Mechanical properties of thin wall ductile iron-influence of carbon equivalent and graphite distribution, ISIJ Int. 44 (2004) 1180–1187.
[4] R.B. Gundlach, J.F. Janowak, Austempered ductile irons combine strength with toughness and ductility, Met. Prog. 128 (1985) 19–26.
[5] A.L. Hitchcox, ADI has what it takes for high-performance gearing, Met. Prog. 130 (1986) 49–51.
[6] R. Harding, Opening up the market for ADI, The Foundryman 86 (1993) 197–208.

[7] R.C. Dommarco, P.C. Bastias, H.A. Dall'O, G.T. Hahn, C.A. Rubin, Rolling contact fatigue (RCF) resistance of austempered ductile iron (ADI), Wear 221 (1998) 69–74.
[8] L. Magalhães, J. Seabra, C. Sá, Experimental observations of contact fatigue crack mechanisms for austempered ductile iron (ADI) discs, Wear 246 (2000) 134–148.
[9] R.C. Dommarco, J.D. Salvande, Contact fatigue resistance of austempered and partially chilled ductile irons, Wear 254 (2003) 230–236.
[10] R.C. Dommarco, A.J. Jaureguiberry, J.A. Sikora, Rolling contact fatigue resistance of ductile iron with different nodule counts and matrix microstructures, Wear 261 (2006) 172–179.
[11] C. Brunetti, M.V. Leite, G. Pintaude, Effect of specimen preparation on contact fatigue wear resistance of austempered ductile cast iron, Wear 263 (2007) 663–668.
[12] J.M. Massone, R.E. Boeri, J.A. Sikora, Changes in the structure and properties of ADI on exposure to high temperature, Int. J. Cast Met. Res. 9 (1996) 79–92.
[13] H.P. Feng, S.C. Lee, C.H. Hsu, J.M. Ho, Study of high cycle fatigue of PVD surface-modified austempered ductile iron, Mater. Chem. Phys. 59 (1999) 154–161.
[14] C.-H. Hsu, J.-K. Lu, R.-J. Tsai, Effects of low-temperature coating process on mechanical behaviors of ADI, Mater. Sci. Eng. A 398 (2005) 282–290.
[15] C.-H. Hsu, M.-L. Chen, K.-L. Lai, Corrosion resistance of TiN/TiAlN-coated ADI by cathodic arc deposition, Mater. Sci. Eng. A 421 (2006) 182–190.
[16] C.-H. Hsu, C.-Y. Lee, K.-L. Chen, J.-H. Lu, Effects of CrN/EN and Cr2O3/EN duplex coatings on corrosion resistance of ADI, Thin Solid Films 517 (2009) 5248–5252.
[17] C.-H. Hsu, K.-L. Chen, K.-C. Lu, Effects of low-temperature duplex coatings on the abrasive and erosive behavior of ADI, Thin Solid Films 519 (2011) 4855–4859.
[18] D.A. Colombo, M.D. Echeverría, O.J. Moncada, J.M. Massone, Characterisation of PVD–TiN coated austempered ductile iron: effects of nodule count and austempering temperature, ISIJ Int. 51 (2011) 448–455.
[19] D.A. Colombo, M.D. Echeverría, O.J. Moncada, J.M. Massone, PVD TiN and CrN coated austempered ductile iron: analysis of processing parameters influence on coating characteristics and substrate microstructure, ISIJ Int. 52 (2012) 121–126.
[20] D.A. Colombo, M.D. Echeverría, O.J. Moncada, J.M. Massone, Residual stress analysis in PVD coated austempered ductile iron, ISIJ Int. 53 (2013) 520–526.
[21] K.J. Martinschitz, R. Daniel, C. Mitterer, J. Keckes, Stress evolution in CrN/Cr coating systems during thermal straining, Thin Solid Films 516 (2008) 1972–1976.
[22] C.J. Smithells, E.A. Brandes, Metals Reference Book, 5th Ed, Butterworths, London, UK, 1976.
[23] M. Zhang, J. He, Ab-initio calculation of elastic constants of TiN, Surf. Coat. Technol. 142-144 (2001) 125–131.
[24] W. Heinke, A. Leyland, A. Matthews, G. Berg, C. Friedrich, E. Broszeit, Evaluation of PVD nitride coatings, using impact, scratch and Rockwell-C adhesion tests, Thin Solid Films 270 (1995) 431–438.
[25] A. Sawamoto, S. Nokubo, Y. Ide, T. Fujita, T. Fukui, K. Yasuoka, Influence of TiN coating on the rolling contact fatigue strength of mild steel, J. Soc. Mater. Sci., Jpn. 45 (1996) 912–918.
[26] P.K. Gupta, J.A. Walowit, Contact stresses between an elastic cylinder and a layered elastic solid, J. Lubr. Technol. 96 (1974) 250–257.
[27] C. Fretigny, A. Chateauminois, Solution for the elastic field in a layered medium under axisymmetric contact loading, J. Phys. D Appl. Phys. 40 (2007) 5418.
[28] R. Kulchytsky-Zhyhailo, G. Rogowski, Stresses in hard coating due to a rigid spherical indenter on a layered elastic half-space, Tribol. Int. 43 (2010) 1592–1601.
[29] B.J. Hamrock, D. Dowson, Isothermal elastohydrodynamic lubrication of point contacts: Part III—Fully flooded results, J. Lubr. Technol. 99 (1977) 264–275.
[30] N.J.M. Carvalho, A.J. Huis in 't Veld, J.T. De Hosson, Interfacial fatigue stress in PVD TiN coated tool steels under rolling contact fatigue conditions, Surf. Coat. Technol. 105 (1998) 109–116.
[31] D. Yonekura, R.J. Chittenden, P.A. Dearnley, Wear mechanisms of steel roller bearings protected by thin, hard and low friction coatings, Wear 259 (2005) 779–788.
[32] T. Sato, T. Saito, S. Fujita, Mechanism of Diamond-Like Carbon (DLC) delamination under rolling contact condition, Tribol. Online 3 (2008) 337–341.
[33] T.S.P. Chang, H.S. Cheng, W.D. Sproul, The influence of coating thickness on lubricated rolling contact fatigue life, Surf. Coat. Technol. 43-44 (1990) 699–708.
[34] H.S. Cheng, T.P. Chang, W.D. Sproul, Proceedings of the 16th Leeds-Lyon Symposium on Tribology, Lyon, France, 1990, pp. 81–88.
[35] T.P. Chang, H.S. Cheng, W.A. Chiou, W.D. Sproul, Comparison of fatigue failure morphology between TiN coated and uncoated lubricated rollers, Tribol. Trans. 34 (1991) 408–416.
[36] I.A. Polonsky, T.P. Chang, L.M. Keer, W.D. Sproul, An analysis of the effect of hard coatings on near-surface rolling contact fatigue initiation induced by surface roughness, Wear 208 (1997) 204–219.